IEEE Access
Multidisciplinary | Rapid Review | Open Access Journal

Received May 15, 2020, accepted June 9, 2020, date of publication June 30, 2020, date of current version July 16, 2020.

Digital Object Identifier 10.1109/ACCESS.2020.3006104

A Novel Traveling Wave Fault Location Method for Transmission Network Based on Directed Tree Model and Linear Fitting

KUN YU[1], JUPENG ZENG[1], XIANGJUN ZENG[1], (Senior Member, IEEE), FAN XU[2], YONG YE[1], AND YANRU NI[1]

[1]School of Electrical and Information Engineering, Changsha University of Science and Technology, Changsha 410114, China
[2]Key Laboratory of Renewable Energy Electric-Technology of Hunan Province, Changsha University of Science and Technology, Changsha 410114, China

Corresponding author: Kun Yu (kunyu0707@163.com)

This work was supported in part by the National Natural Science Foundation of China under Grant 51807012, and in part by the Key Laboratory of Renewable Energy Electric-Technology of Hunan Province, Changsha University of Science and Technology.

ABSTRACT In order to solve the problem of inaccurate fault location in the transmission network under some abnormal conditions, such as traveling wave location device faults, startup failure and time recording error, a novel traveling wave fault location method based on directed tree model and linear fitting is proposed. A directed tree model of the fault traveling wave transmission along the shortest path is established based on graph theory analysis of traveling wave transmission network. Two straight lines are fitted on the coordinate plane where the accurate fault location is obtained direct by coordinate information of the intersection of these two fitted straight lines (FSLs), according to the transmission characteristics of the fault traveling wave in the directed tree model. The wave velocity is used as the slope of the fitted straight line, and the influence of its uncertainty on the fault location is eliminated. The time record error points of the location device are automatically eliminated in the linear fitting. PSCAD simulation results prove that fault information of the entire transmission network is comprehensively utilized by the proposed method and the ring network is automatically unlooped. The reliability and accuracy of fault location are remarkably improved, particularly for the fault scenarios with recorded information abnormity.

INDEX TERMS Transmission network, fault location, traveling wave, directed tree model, linear fitting.

I. INTRODUCTION

With the rapid development of smart grids, the capacity of power systems and the area of power grids are constantly being expanded, resulting in more complicated power grid operation management [1], [2]. The fault location is quickly and accurately determined after a transmission line failure, which not only reduce the burden of patrolling the line and repair the line in time to achieve the purpose of ensuring reliable power supply, but also reduce the overall economic loss caused by power outages. Therefore, high-precision power grid fault location is of great significance to the safety, stability, and economic operation of the power system [3], [4]. At the same time, a method of strong anti-interference ability and comprehensive use of the entire network fault information for fault location is very necessary for fault location of the transmission network.

The location of fault points of high-voltage transmission lines is generally realized by the impedance method and injection method. However, the practical application of impedance method is not ideal, because its measurement accuracy is affected by factors such as fault resistance, transformer errors, asymmetry of the line structure, and uneven distribution of zero-sequence parameters along the line [5], [6]. Injection method for fault location is more targeted than manual line patrol to find fault points. However, this method requires new equipment, high cost, and the strength of the injected signal is difficult to grasp [7], [8]. Various fault location methods for transmission networks are proposed by scholars at home and abroad with the continuous progress of computer, communication and measurement technology. Among them, a large number of fault location methods based on the traveling wave principle are widely

The associate editor coordinating the review of this manuscript and approving it for publication was Flavia Grassi.

used in power transmission networks, because they are applied to transmission lines with a variety of structures, different transition resistances and different parameters [9]. The traditional single-ended traveling wave location principle is simple to implement and highly reliable [10], [11]. However, it is very difficult to accurately identify the nature of the reflected traveling wave due to the interference of the complex ring network structure of the transmission network. Compared with the single-ended method, the currently used two-terminal traveling wave location method is not affected by various reflected waves and refracted waves, because it only needs to capture the first fault traveling wave head that arrives both ends of the transmission line [12]–[14]. In some existing two-terminal traveling wave location methods, generally only fault information is considered on one or both sides of the line [15]–[17]. Fault information on the entire network is not fully utilized, and the accuracy and reliability of fault location needs to be improved. Based on this, the literatures [18], [19] propose that synchronous measurement devices are set at the head and end of each transmission line in the transmission network, so the two-terminal method is extended to a multi-terminal method, which obtains a relatively good location effect. A new principle of two-terminal traveling wave location technology is proposed in [17]–[19], which uses the travel time difference between the aerial modal and ground modal to calculate the fault distance of the transmission line. However, these methods have higher requirements for the accuracy of ground-mode wave velocity extraction, and their practical applications need to be explored. In literature [20], a novel fault section identification method that depends only on the first three arrival times is applied to separate a three-terminal fault section from the multi-terminal lines. Consequently, the fault is located using a corresponding two-terminal fault location method in this fault section, but the high accuracy of the traveling wave arrival time measurement is required in this method whose application effect is not ideal when there is a time recording error. In order to eliminate the impact of time recording errors of a certain location device in the entire transmission network, the methods of [21]–[23] are proposed. The complex structure of a multi-terminal power system is divided into several fault identification branches with an algorithm proposed in [21], where the current at the midpoint of each branch is measured to eliminate time recording errors, but this algorithm needs to calculate the time difference for faults in various intervals so the amount of calculation is large. Later the location algorithm based on neural network and network path is proposed in [22] and [23], respectively, where the algorithm and fault information judgment are all improved, but time data fusion is still not improved. In addition, in the above methods, only the radiation type transmission network is considered, and the existence of a ring network is not considered. Some transmission network location methods based on calculating the shortest path of traveling wave transmission to realize the ring network to be automatically unlooped are proposed in literature [24]–[26]. These methods have been well applied in practical transmission networks, but in order to improve the reliability of the data during data processing, weighting is used to calculate the fault distance, where the weights are set based only on the distance of each traveling wave detection device from the fault point. However, distant information with high time accuracy is ignored by this weighting process, and more human factors are introduced.

To solve these problems, a novel traveling wave fault location method based on directed tree model and linear fitting is proposed in this paper. By analyzing the transmission characteristics of the fault traveling wave, a directional tree model composed of the shortest path directional tree is established, which contains two sets of related data for linear fitting. The intersection of two straight lines fitted using two sets of data is the fault distance, according to the characteristic that the traveling wave head arrival time recorded by the traveling wave location device of each substation is linearly proportional to the relative distance between each substation. Simulation results show that the fault information of the entire transmission network is comprehensively utilized, the influence of wave velocity uncertainty and fault traveling wave time recording error on traveling wave location accuracy is eliminated, and ring network is automatically unlooped by the proposed method to realize fast and accurate location.

II. ESTABLISHMENT OF DIRECTED TREE MODEL

A. ANALYSIS OF FAULT TRAVELING WAVE TRANSMISSION CHARACTERISTICS

A fault traveling wave is transmitted to both ends of the line starting from the fault location, when a fault occurs on a certain line of the transmission network. An intricate traveling wave transmission network is formed in the entire power grid, because the fault traveling wave is refracted and reflected at the discontinuous location of the wave impedance such as the location of the detection point. The fault initial traveling wave is the first fault traveling wave signal detected by each traveling wave location device after the fault occurs. The traveling wave location device installed at the bus bar and substation is used to record the fault initial traveling wave, because it travels along the shortest path, with less refraction and reflection, small energy attenuation, obvious fault feature quantity, and easy to extract and detect. The fault feature quantity such as wave head arrival time contained in the traveling wave signal is extracted to achieve the purpose of accurate fault location.

Figure 1 depicts a typical topology structure for transmission network of traveling wave. The propagation direction and path of the fault initial traveling wave in the transmission network are shown in Figure 1, where the time marked on this figure is the time when the initial traveling wave arrives at each substation, and the solid arrow indicates the propagation path of the fault traveling wave. The arrival time of the fault initial traveling wave only needs to be accurately recorded to

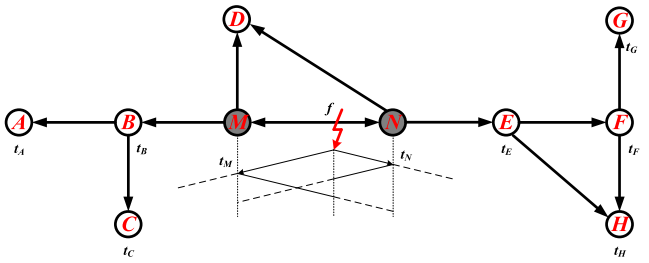

FIGURE 1. Topology structure for transmission network of traveling wave.

achieve fault location, according to the method proposed in this paper.

B. DEFINITION OF SHORTEST PATH DIRECTED TREE

In graph theory, a tree is a finite set of n ($n \geq 0$) nodes and b ($b \geq n$) branches, the tree is called an empty tree, when $n = 0$, otherwise it is called a non-empty tree. Any non-empty tree has the following characteristics:

(1) The fault point in the transmission network is called the root node of the tree.

(2) The other nodes except the root node are divided into multiple disjoint sets, where each set is a branch and is called a subtree of the tree.

(3) A tree with a direction is called a directed tree.

The shortest path directed tree is proposed to analyze the traveling wave transmission network based on graph theory, according to the research on traveling wave transmission characteristics in Section II.A. The fault point f is defined as the root node of the tree, and points M and N are defined as subtree root nodes, as shown in Figure 2. The shortest path transmitted by traveling wave from the fault point f is equivalent to the shortest path transmitted by M and N to the left and right ends, respectively. The shortest paths from two subtree root nodes to other nodes are obtained according to Dijkstra algorithm [27]. Let V denote the set of nodes, which corresponds to the set of substations or buses in the transmission network, and let E denote the set of branches, which corresponds to the set of transmission lines. The specific algorithm steps are as follows:

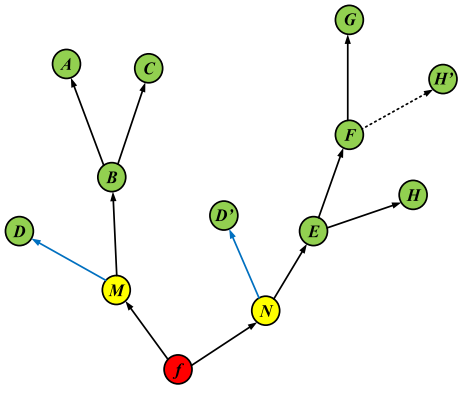

FIGURE 2. The directed tree model of the fault initial traveling wave.

Step 1: Initialize sets V and E, and define the set S which contains only the fault point f at this time.

Step 2: Select the point i closest to the fault point f from the set V and add it to the set S.

Step 3: Take point i as the new intermediate point to re-consider the shortest path of other points, and modify the distance of each point in the set V.

Step 4: If the distance from the fault point f via point i to point i' ($i' \in V$) is shorter than the distance from $f \rightarrow i'$, then modify the distance from point i'. The modified distance should be the distance from $f \rightarrow i \rightarrow i'$.

Step 5: Repeat steps 2, 3, and 4 until all points in the set V are included in the set S.

The shortest path set from the subtree root node M to its left points is defined as L_M, and the shortest path set from the subtree root node N to its right points is also defined as L_N, after the shortest path is obtained through the Dijkstra algorithm. Therefore, a directed tree that is not the shortest path is eliminated in Figure 2, and the results of L_M and L_N are as follows:

$$\begin{cases} L_M = \{l_{MA}, l_{MB}, l_{MC}, \ l_{MD}\} \\ L_N = \{l_{ND}, l_{NE}, l_{NF}, \ l_{NG}, l_{NH}\} \end{cases} \tag{1}$$

where l_{Mi} ($i = A, B, C, D$) is the shortest path from M to the point on its left; l_{Nj} ($j = D, E, F, G, H$) is the shortest path from N to the point on its right.

Combining Figure 1 and Figure 2, the topology of the transmission network is defined as follows:

(1) Any subtree root node is selected as the distance base point (DBP).

(2) The initial traveling wave which propagates along the DBP toward the root node (fault point) is defined as the positive direction traveling wave (PDTW) and the wave velocity is positive, otherwise it is the negative direction traveling wave (NDTW) and the wave velocity is negative.

(3) The substation passing by the PDTW is defined as the positive direction substation (PDS) and the distance from the DBP is positive, otherwise it is the negative direction substation (NDS) and the distance from the DBP is negative.

If subtree root node M is selected as the DBP as shown in Figure 1, substations A, B, C and D are NDSs, and substations D, E, F, G and H are PDSs. D is either PDS or NDS due to the special nature of the fault occurring in the ring network. From Equation (1), the transmission distance between PDS and DBP is:

$$L_+ = L_N + l_{MN} \tag{2}$$

where l_{MN} is the distance between point M and point N via fault point f. From Equation (1), the transmission distance between NDS and DBP is:

$$L_- = -L_M \tag{3}$$

C. DEFINITION OF VIRTUAL TREE

There are ring networks MND and EFH in the transmission network as shown in Figure 1. In case of fault in a ring

network, the shortest path of the initial traveling wave transmission needs to be judged, because the fault traveling wave start from the fault point to reach point D through M ($f \rightarrow M \rightarrow D$), and also reach point D through N ($f \rightarrow N \rightarrow D$). The interference line existing in this judgment process is defined as a virtual tree, so the shortest path directed tree suitable for the ring network is established. The specific steps are as follows:

Step 1: Unloop the ring network at points D and H, and add subtree nodes D' and H'.

Step 2: Create the shortest path directed tree according to the method in Section II.B.

Step 3: Judge points D and H to exclude wrong virtual trees.

There is no virtual tree at point H and the $H'F$ path should be eliminated in the directed tree model, because point H is fixed and unique based on the Dijkstra algorithm when seeking the shortest path. Point D cannot determine the shortest path for traveling waves transmission, so MD and ND' are defined as virtual trees. Virtual trees are represented by blue lines in Figure 2. Ring network is automatically unlooped by this proposed method, because the virtual points corresponding to the wrong virtual tree are automatically eliminated by the linear fitting criterion used in the later paper content.

III. FAULT LOCATION METHOD BASED ON LINEAR FITTING AND DIRECTED TREE MODEL

A. ANALYSIS OF FITTED STRAIGHT LINES FOR FAULT TRAVELING WAVES

The fault initial traveling wave arrival time of each substation recorded in the transmission network is linearly proportional to the transmission distance (linear function form is $Y = aX + b$), according to the principle of traveling wave transmission. The fitted straight line (FSL) that directly represents the traveling wave transmission characteristics is obtained based on the principle of univariate linear regression. Accurate fault location is directly realized, according to the fault characteristics displayed by the fault point on the FSL.

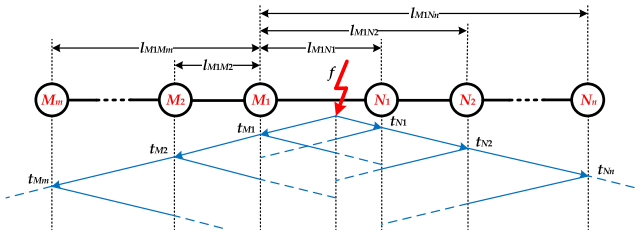

FIGURE 3. Topology structure of the shortest path of the transmission network.

The fault occurs at the line M_1N_1 in the shortest path topology of the transmission network shown in Figure 3. Taking the substation M_1 as the DBP, any substation in this transmission network is defined as k which is:

$$k = \begin{cases} M_i (i = 1, 2, \ldots, m), & \text{if } k \text{ located on the left of } f \\ N_j (j = 1, 2, \ldots, n), & \text{if } k \text{ located on the right of } f \end{cases} \tag{4}$$

For any substation k on the left side of the fault point f, there must be:

$$l_{M_1 k} = v(t_k - t_{M_1}) = vt_k - vt_{M1} \tag{5}$$

where v is the traveling wave propagation velocity; l_{M1k} is the shortest path from M_1 to any substation k; t_{M1} is the initial traveling wave arrival time recorded at detection point M_1; t_k is the initial traveling wave arrival time recorded at any detection point k. Similarly, for any substation k on the right side of the fault point f, there must be:

$$l_{M_1 k} = v(t_k - t_{N_1}) + l_{M_1 N_1} = vt_k - vt_{N_1} + l_{M_1 N_1} \tag{6}$$

where t_{N1} is the initial traveling wave arrival time recorded at detection point N_1; l_{M1N1} is the distance between point M_1 and point N_1 via fault point f.

Observing Equations (5) and (6), which are linearly fitted according to the principle of univariate linear regression. Let $Y = l_{M1k}, X = t_k$. From Equation (5), $a_1 = v, b_1 = -vt_{M1}$, and $Y = a_1 X + b_1$. From Equation (6), $a_2 = v, b_2 = -vt_{N1} + l_{M1N1}$, and $Y = a_2 X + b_2$. The values of a_1 and a_2 that are both wave speeds v, should be equal according to the above analysis, but a_1 and a_2 can only be approximately equal, because the slopes of two straight lines fitted through two sets of different data are somewhat different based on the perspective of linear fitting. The minimum of Equation (7) are obtained by the a_1, a_2, b_1 and b_2 parameters, according to the principle of univariate linear regression.

$$\begin{cases} Q(a_1, b_1) = \sum_{i=1}^{m} (l_{M_1 k(i)} - a_1 - b_1 t_{k(i)})^2 \\ Q(a_2, b_2) = \sum_{j=1}^{n} (l_{M_1 k(j)} - a_2 - b_2 t_{k(j)})^2 \end{cases} \tag{7}$$

where $k(i) = M_i$ ($i = 1, 2, \ldots, m$), $k(j) = N_j$ ($j = 1, 2, \ldots, n$). From the minimum value, the a_1, a_2, b_1 and b_2 parameters should be satisfied by the following Equations (8) and (9):

$$\begin{cases} \dfrac{\partial Q}{\partial a_1} = -2 \sum_{i=1}^{m} \left(l_{M_1 k(i)} - a_1 - b_1 t_{k(i)} \right) = 0 \\ \dfrac{\partial Q}{\partial b_1} = -2 \sum_{i=1}^{m} \left(l_{M_1 k(i)} - a_1 - b_1 t_{k(i)} \right) t_{k(i)} = 0 \end{cases} \tag{8}$$

$$\begin{cases} \dfrac{\partial Q}{\partial a_2} = -2 \sum_{j=1}^{n} \left(l_{M_1 k(j)} - a_2 - b_2 t_{k(j)} \right) = 0 \\ \dfrac{\partial Q}{\partial b_2} = -2 \sum_{j=1}^{n} \left(l_{M_1 k(j)} - a_2 - b_2 t_{k(j)} \right) t_{k(j)} = 0 \end{cases} \tag{9}$$

Equations (8) and (9) are simplified, and the values of a_1, a_2, b_1 and b_2 are solved as follows:

$$\begin{cases} a_1 = \dfrac{\sum_{i=1}^{m} l_{M_1k(i)} - b_1 \sum_{i=1}^{m} t_{k(i)}}{m} \\ b_1 = \dfrac{m\sum_{i=1}^{m} l_{M_1k(i)}t_{k(i)} - \sum_{i=1}^{m} l_{M_1k(i)} \sum_{i=1}^{m} t_{k(i)}}{m\sum_{i=1}^{m} t_{k(i)}^2 - (\sum_{i=1}^{m} t_{k(i)})^2} \end{cases} \tag{10}$$

$$\begin{cases} a_2 = \dfrac{\sum_{j=1}^{n} l_{M_1k(j)} - b_2 \sum_{j=1}^{n} t_{k(j)}}{n} \\ b_2 = \dfrac{n\sum_{j=1}^{n} l_{M_1k(j)}t_{k(j)} - \sum_{j=1}^{n} l_{M_1k(j)} \sum_{j=1}^{n} t_{k(j)}}{n\sum_{j=1}^{n} t_{k(j)}^2 - (\sum_{j=1}^{n} t_{k(j)})^2} \end{cases} \tag{11}$$

FSL1 ($Y = a_1X + b_1$) corresponding to Equation (5) and FSL2 ($Y = a_2X + b_2$) corresponding to Equation (6) are calculated by Equation (10) and Equation (11), respectively. The FSL1 and FSL2 are obtained as shown in Figure 4.

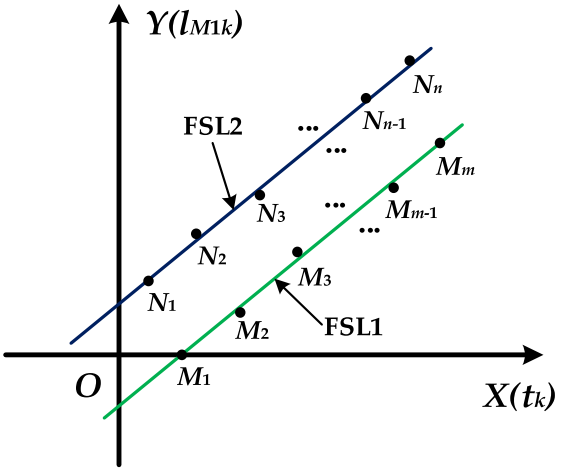

FIGURE 4. Linear fitting graph of fault traveling wave.

B. FAULT LOCATION ALGORITHM BASED ON INTERSECTION OF FITTED STRAIGHT LINES

Based on the definition of the directional tree in section II.B and the analysis of linear fitting in section III.A, point M_1 is set as the DBP in the transmission network shown in Figure 3. The traveling wave propagating to the right from the fault point f is PDTW, the wave velocity is positive, and $N_1, N_2, \ldots, N_n$ are PDSs whose distances from the DBP are positive. On the contrary, the traveling wave propagating to the left from the fault point f is NDTW, the wave velocity is negative, and $M_1, M_2, \ldots, M_m$ are the NDSs whose distances from the DBP are negative. At this time, equations (5) and (6) are still satisfied by all the substations in Figure 3, but the wave velocity is changed from scalar to vector.

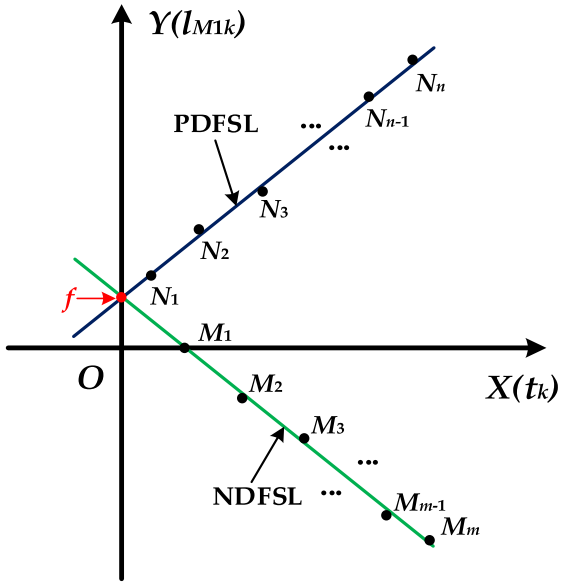

FIGURE 5. Schematic diagram of fault location method.

In Figure 4, the slope of the FSL1 is changed from $+v$ to $-v$ (from a_1 to $-a_1$) and the intercept of the FSL1 is changed from $-vt_{M1}$ to $+vt_M$(from b_1 to $-b_1$), according to the above definition and analysis. FSL1 and FSL2 have a unique intersection point f that is caused by this change as shown in Figure 5. According to the physical meaning of the FSL of the fault traveling wave, the intersection point f must be the fault point, because only the traveling wave at the fault point is propagated in two different directions of the fault line in a transmission network, where the propagation direction of the traveling wave at point f is both positive and negative. Therefore, FSL1 and FSL2 are defined as a negative direction fitted straight line (NDFSL) and a positive direction fitted straight line (PDFSL), respectively. The ordinate of the intersection point f of the two straight lines represents the fault distance between the fault point f and the DBP M_1. The ordinate of the intersection of PDFSL and NDFSL is solved by following simultaneous Equation (12):

$$\begin{cases} Y = -a_1X - b_1 \\ Y = a_2X + b_2 \end{cases} \tag{12}$$

where the values of a_1, a_2, b_1, and b_2 are calculated by Equations (10) and (11). Therefore, accurate location of transmission network faults is achieved through this fault distance which is calculated by Equation (13):

$$l_{M_1f} = Y_f = \frac{a_1b_2 - a_2b_1}{a_1 + a_2} \tag{13}$$

Compared with the traditional traveling wave location algorithm, a rectangular coordinate system which represents the fault traveling wave transmission characteristics is established by the algorithm in this paper, where the fault information of the entire transmission network is comprehensively utilized. In rectangular coordinate system,

the influence of wave velocity as the slope of FSL on fault location is automatically eliminated, and accurate fault location is achieved according to the intersection of PDFSL and NDFSL. The proposed algorithm is easy to implement and apply in practical power systems, because it is simple and does not require a complicated solution process.

C. CORRECTION CRITERIA FOR FITTING STRAIGHT LINES

Incorrect fault traveling wave recording time is automatically eliminated by the fault location algorithm based on intersection of fitted straight lines in this paper, so the proposed algorithm is not affected by a certain point of equipment fault or synchronization time error. In order to improve the location accuracy of the algorithm, however, two correction criteria for fitting straight lines are proposed in this paper to ensure the high accuracy of the FSLs and realize the error-free description of the fault traveling wave transmission characteristics.

Correction criterion 1: The fitting time value t_k' and the actual recording time value t_k of the fault traveling wave arrival time of each substation are corrected one by one. The time synchronization error is realized as 1μs, according to the synchronized second clock developed by the author's research group. The error between the fitting time value t_k' and the actual recording time value t_k of each substation should be less than 1μs, because to ensure that the fault location error is less than 150m [28], that is, all PDSs and NDSs must be satisfied by the Equation (14):

$$\left|t_k' - t_k\right| \leq 1\mu\text{s} \tag{14}$$

Correction criterion 2: Although traveling waves have certain dispersion characteristics and traveling wave components of different frequencies have different propagation velocities when they are transmitted on the transmission line, the deviation of the traveling wave velocity from the velocity of light is small, according to the transmission characteristics of traveling waves. Based on the above analysis, the slopes of the two straight lines fitted by the proposed algorithm must be satisfied by the Equation (15):

$$\left|\frac{|a|}{v_{light}} - 1\right| \times 100\% \leq 1\% \tag{15}$$

where v_{light} is the velocity of light which is about 0.3km/μs; a is $-a_1$ or a_2 which are calculated from Equation (10) or Equation (11), respectively.

Therefore, after obtaining PDFSL and NDFSL in Section III.B, first of all, the fitting result is corrected by the correction criterion 1, where the fitting points that do not satisfy the Equation (14) are eliminated, and then the linear fitting is performed again. Secondly, the slope of the FSL is corrected according to the correction criterion 2. If the slope is satisfied by Equation (15), the accuracy requirement of the fitting result is satisfied, otherwise, the FSL needs to be refitted. Finally, if the FSL has been fit for many times, the correction criterion 1 and the correction criterion 2 still cannot be satisfied, then the proposed algorithm is invalid.

The fitting error points are automatically eliminated through the linear fitting process of the proposed algorithm, which is equivalent to eliminating errors caused by factors such as traveling wave location device faults, startup failure and time recording error. Based on this principle, when a fault occurs in a ring network, the fault traveling wave arrival time (wrong virtual tree) that is not the shortest transmission path during linear fitting is automatically eliminated by the proposed algorithm, because the fault traveling wave transmission path in the ring network is not unique. Therefore, the linear relationship between the transmission time and the transmission distance of the traveling wave is quantitatively described, and the ring network is automatically unlooped to achieve reliable and accurate fault location.

IV. IMPLEMENTATION OF THE PROPOSED FAULT LOCATION METHOD

The implementation steps of the proposed fault location method are shown in Figure 6, when a fault occurs at any point on a certain line. The detailed steps are as follows: where EMS stands for Energy Management System.

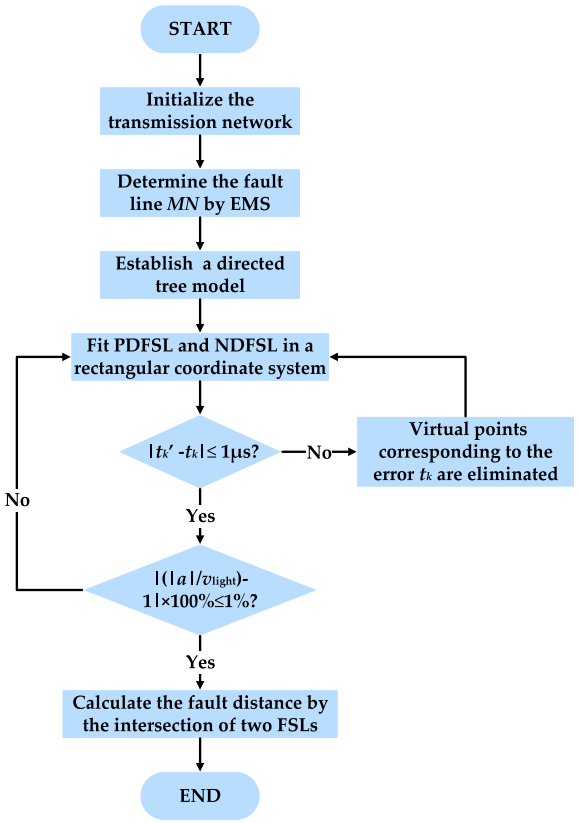

FIGURE 6. Flowchart of the proposed fault location method.

Step 1: The network parameters, including substation parameters, transmission line parameters, switching parameters, and serial numbering of the end of the network at each detection point, are initialized. Among them, the transmission line length is obtained by the following methods: the traveling wave signal is generated by using the opening and closing of each circuit breaker of the line to measure the length of each

section of the line, after the installation of the traveling wave location system is completed.

Step 2: The status of the circuit breaker is obtained, according to the Energy Management System (EMS), and the fault line is judged. The fault line MN is connected to the substation with the initial traveling wave arrival time and tripped.

Step 3: The directed tree model is established by the Dijkstra algorithm, where the DBP, PDTW, NDTW, PDS and NDS, are determined. The values of L_+ and L_- are calculated by Equations (2) and (3), and the initial traveling wave arrival time of each substation is detected.

Step 4: The positive and negative data obtained in step 3 are used, in which the shortest path from the PDS to the DBP is positive and the shortest path from the NDS to the DBP is negative. The time when the initial traveling wave arrives at each substation is taken as the X axis, and the shortest path between each substation and the DBP is taken as the Y axis to establish a rectangular coordinate system, where the two straight lines PDFSL and NDFSL are drawn after the linear fitting.

Step 5: Each positive and negative data point is judged whether it is satisfied by the correction criterion 1, and the virtual data points not satisfied by the Equation (14) are eliminated.

Step 6: The slopes of the two fitted straight lines are judged whether it is satisfied by the Equation (15) of the correction criterion 2. If yes, go to step 7, otherwise go to step 4.

Step 7: The fault distance is calculated by Equation (13), according to the ordinate of the intersection of the two straight lines, the final PDFSL and NDFSL, to achieve accurate and reliable fault location.

V. SIMULATION ANALYSIS

A. SIMULATION MODEL

The PSCAD/EMTDC is employed to test the proposed fault location method. The simulation model is a typical Chinese 500kV transmission network whose topology is shown in Figure 7. There are 10 substations and 14 transmission lines, whose tower configuration and parameters are given in Figure 8 and Table 1, respectively. All transmission lines are modeled by frequency-dependent line model, with the same conductor for type LGJ-300/40 and the same ground wire for type GJ-100. The maximum sags of all conductors and ground wires are 13.50m and 11.25m, respectively. The earth resistivity is 250Ω/m and the length of each transmission line is marked in Figure 7 (the unit is km).

In the simulation model, set A-phase-to-ground (AG) fault point f_1 with a transition resistance of 50Ω, which is located on the line CD, and is 26.95km away from the point C. Set AB-phase-to-ground (ABG) fault point f_2 with a transition resistance of 100Ω, which is located on the line EF, and is 39.53km away from the point E. Set BC-phase-to-phase (BC) fault point f_3 with a transition resistance of 200Ω, which is located on the line IG, and is 68.74km away from the point I.

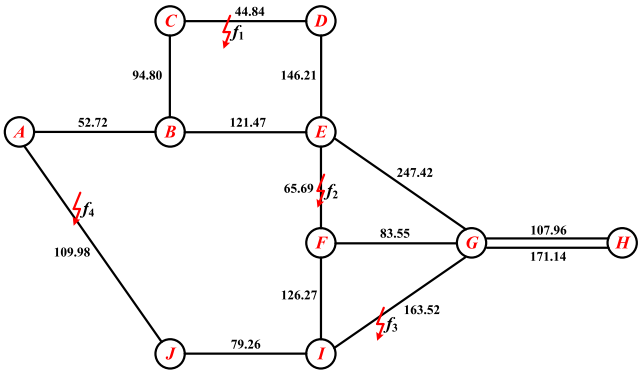

FIGURE 7. Simulation topology model for 500kV transmission network.

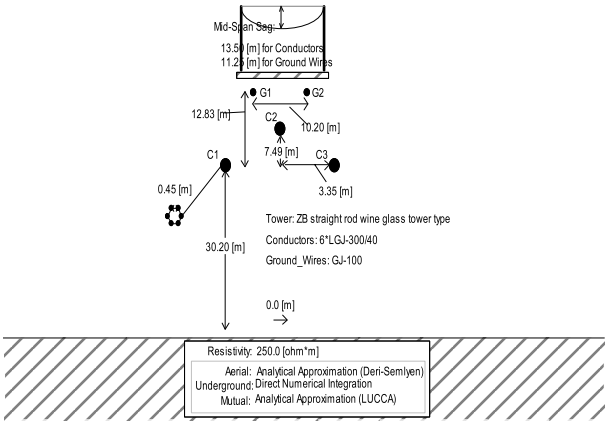

FIGURE 8. Configuration of the 500kV transmission line tower.

Set C-phase-to-ground (CG) fault point f_4 with a transition resistance of 400Ω, which is located on the line AJ, and is 85.31km away from the point A.

TABLE 1. Parameters of the 500kV transmission line for simulation.

Parameter Type	r (Ω/km)	x (Ω/km)	g (s/km)	b (s/km)
Positive Sequence	0.01986	0.19468	1×10^{-7}	3.271×10^{-6}
Zero Sequence	0.16381	1.19621	1×10^{-7}	2.323×10^{-6}

B. DETECTION OF FAULT INITIAL TRAVELING WAVE ARRIVAL TIME AT EACH SUBSTATION

The accurate detection of fault initial traveling wave arrival time at each substation is important for fault location. In this paper, synchronous detection devices are set at the head and end of each line to collect voltage signals by the coupling capacitor voltage transformers (CCVT) at a sampling frequency of 10MHz [29]. The Karenbauer transformation is applied for transforming the coupled three-phase voltage components to independent modal components including the ground and aerial modal components. The Karenbauer transformation is given as [30], [31]:

$$\begin{bmatrix} u_\alpha \\ u_\beta \\ u_\gamma \\ u_0 \end{bmatrix} = \frac{1}{3} \begin{bmatrix} 1 & -1 & 0 \\ 1 & 0 & -1 \\ 0 & 1 & -1 \\ 1 & 1 & 1 \end{bmatrix} \begin{bmatrix} u_a \\ u_b \\ u_c \end{bmatrix} \tag{16}$$

where u_a, u_b and u_c represent the three-phase voltages, respectively; u_α, u_β and u_γ represent the aerial-mode voltages; u_0 represents the ground-mode voltage. The aerial modal component is more suitable for fault location than the ground modal component, because the ground modal traveling wave head attenuation is severe and difficult to detect. Therefore, u_α is selected to obtain the detection of fault initial traveling wave arrival time at each substation.

In order to better identify the wave head of the fault initial traveling wave to obtain accurate time, u_α needs to be decomposed by wavelet transform. Daubechies-4 (db4) Discrete Wavelet Transform (DWT) is used to transform the transient voltage samples based on the research of traveling wave transmission paths because of its prominent characteristic of time-translation invariance. The first peak shown in the detail-1 signal of the DWT is corresponding to the arrival time of the fault initial traveling wave at the detection device, which are obtained by observing wavelet transformation coefficient squared (WTC^2s). The DWT of discrete signal $f[n]$ is quickly implemented by the Mallat algorithm [32], [33]:

$$\begin{cases} V_{2^j}f[n] = \sum_k h[k]V_{2^{j-1}}f[n-2^{j-1}k] \\ W_{2^j}f[n] = \sum_k g[k]V_{2^{j-1}}f[n-2^{j-1}k] \end{cases} \tag{17}$$

where $V_2^j f[n]$ and $W_2^j f[n]$ are the low-frequency approximation coefficients and the high-frequency detail coefficients in scale j, respectively. The approximation coefficients in scale 0 is exactly the original discrete signal $f[n]$. $h[n]$ and $g[n]$ are the low-pass and high-pass filter coefficients, respectively, corresponding to the selected mother wavelet.

The above four fault points are simulated separately, and the time when the fault initial traveling wave arrives each substation is obtained after Karenbauer transformation and DWT, as shown in Table 2. Taking the simulation result of the fault point f_1 as an example, this paper shows the waveform diagram of fault traveling wave u_α signals at each substation and their WTC^2s results, as shown in Figure 9 and Figure 10, respectively. The abscissa corresponding to the first peak in Figure 10 is the time when the fault initial traveling wave arrives each substation.

TABLE 2. Arrival times of fault initial traveling wave head.

Site Name	Arrival Time (μs)			
	f_1	f_2	f_3	f_4
A	582.1	713.1	860.7	284.6
B	406.2	537.2	1036.7	460.5
C	89.9	769.3	1353.0	776.8
D	59.7	619.7	1302.0	926.4
E	547.5	131.9	814.1	865.9
F	766.6	87.3	595.0	768.0
G	1045.4	366.0	316.2	892.3
H	1405.6	726.2	676.4	1252.5
I	1187.9	508.5	229.4	346.7
J	949.1	772.9	493.7	82.3

C. TYPICAL CASE ANALYSIS OF PROPOSED METHOD

1) TEST CASE 1: AG FAULT f_1

In the first case, the AG fault f_1 shown in Figure 7 occurs on the line *CD*. Point *C* is selected as the DBP, and the direction of the wave velocity when the traveling wave is transmitted from the fault point f_1 to point *D* is set to the positive direction, according to the analysis in Section II. A directed tree model for fault f_1 as shown in Figure 11 is established. In order to verify that the time recording of the traveling wave location device of a substation in the transmission network is incorrect, the proposed method can still accurately locate the fault. It is assumed that the traveling wave location device of the substation *G* records the error time which is 926.8μs. In the actual situation, the time recording error of the location device may be due to the interference of some random errors. The traveling wave arrival time of each substation and its distance from the DBP are recorded according to this model, where the NDSs data and PDSs data are shown in Tables 3 and 4, respectively.

According to the data in Tables 3 and 4 and the linear fitting principle, the initial traveling wave head arrival time is taken as the X axis, and the distance from each substation to the DBP is taken as the Y axis, two FSLs called PDFSL and NDFSL are plotted in this rectangular coordinate system, as shown in Figure 12. The straight line equation of the two FSLs is calculated by the principle of univariate linear regression as follow:

$$\begin{cases} Y = -0.29971X + 26.94388 \\ Y = 0.29972X + 26.95840 \end{cases} \tag{18}$$

where $a_1 = 0.29971$, $a_2 = 0.29972$, $b_1 = -26.94388$ and $b_2 = 26.95840$.

In linear fitting, the error point *G* and the virtual point *I* are eliminated according to the correction criterion 1:

$$\begin{cases} |t'_G - t_G| = |1045.4 - 926.8|\,\mu s = 118.6\mu s \geq 1\mu s \\ |t'_I - t_I| = |1213.5 - 1187.9|\,\mu s = 25.6\mu s \geq 1\mu s \end{cases} \tag{19}$$

where t_G' and t_I' are the fitting times of the fault traveling waves to the subtree nodes *G* and *I*, respectively. So that the incorrect virtual tree *JI* is eliminated, and the ring network is automatically unlooped. At this time, the slopes of the two fitted straight lines are satisfied by correction criterion 2:

$$\begin{cases} \left|\dfrac{|-a_1|}{v_{light}} - 1\right| \times 100\% = \left|\dfrac{|-0.29971|}{0.3} - 1\right| \\ \qquad \times 100\% = 0.097\% \leq 1\% \\ \left|\dfrac{|a_2|}{v_{light}} - 1\right| \times 100\% = \left|\dfrac{|0.29972|}{0.3} - 1\right| \\ \qquad \times 100\% = 0.093\% \leq 1\% \end{cases} \tag{20}$$

The location of the fault point is the intersection of two fitted straight lines. According to the Equations (13) and (18), the fault distance $l_{Cf1} = 26.95114$km. The location error of this case is 0.003%. The main theoretical error may come from two aspects: On the one hand, it is related to the error of the linear fitting in the fitting accuracy. Therefore, it is only

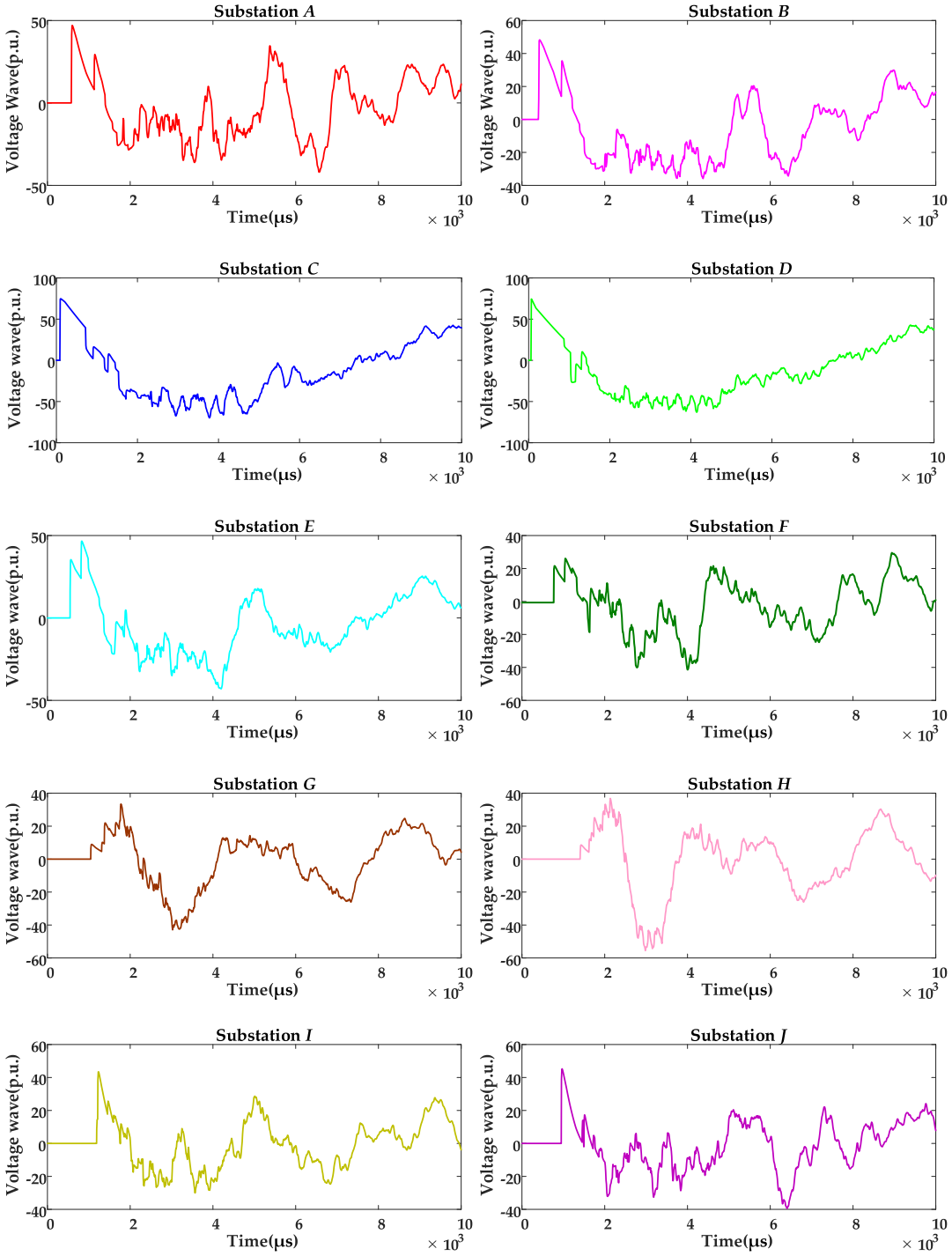

FIGURE 9. Voltage traveling wave u_α signals at each substation for AG fault f_1.

necessary to ensure that the points of the linear fitting are correct, then the error of fitting the straight line is very small, and it will basically not affect the fault location. On the other hand, it is related to the correction criterion proposed by the authors. According to the basic principle that the traveling wave velocity is close to the velocity of light, the authors set the difference between the error time and the fitting time to $1\mu s$ in the correction criterion. This setting can control the location error within 150m, which greatly reduce the impact of time recording error points on fault location.

2) TEST CASE 2: ABG FAULT f_2

In the second case, the ABG fault f_2 shown in Figure 7 occurs on the line EF. Point E is selected as the DBP, and

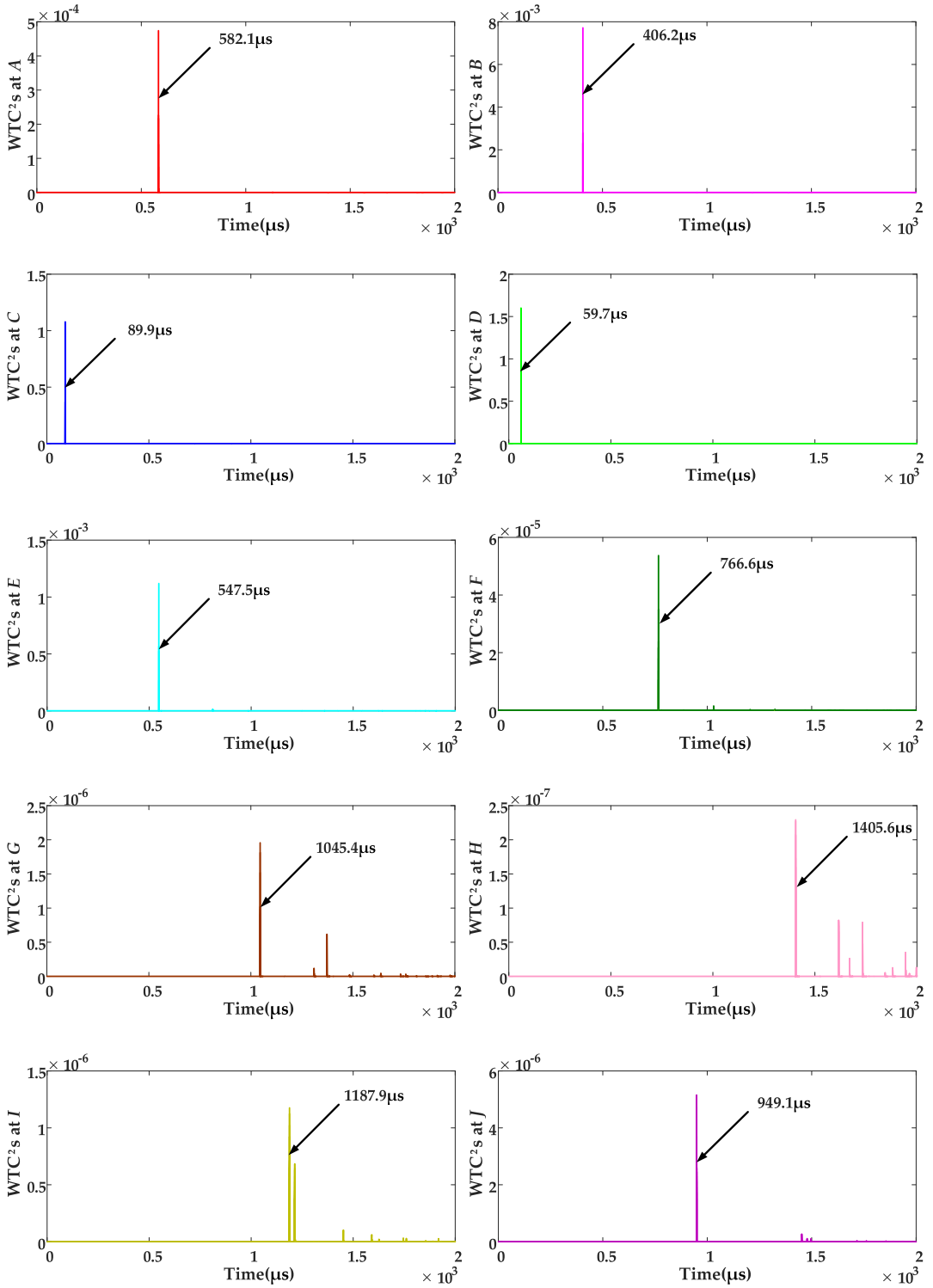

FIGURE 10. Arrival time at each substation obtained by voltage WTC^{2}s for AG fault f_1.

the direction of the wave velocity when the traveling wave is transmitted from the fault point f_2 to point F is set to the positive direction. A directed tree model for fault f_2 as shown in Figure 13 is established. Any one of the location devices may malfunction and start failure in actual operation, resulting in the situation that the substation cannot detect the traveling wave signal. Assume that, the traveling wave location device of the substation H fails or fails to start, which causes the arrival time of the traveling wave signal is not recorded. At this time, the traveling wave location device of

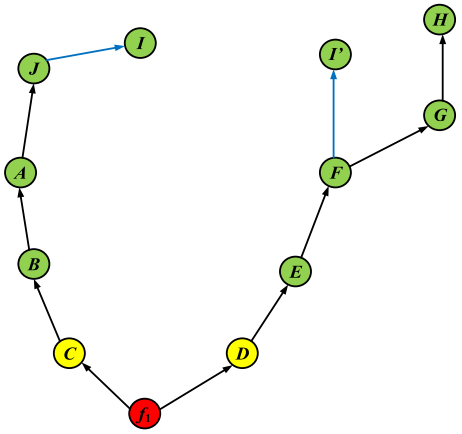

FIGURE 11. Directed tree model for fault f_1.

TABLE 3. Data for the NDSs of fault f_1.

NDS Name	t_k (μs)	L_- (km)
A	582.1	-147.52
B	406.2	-94.80
C	89.9	0
I	949.1	-257.50
J	1187.9	-336.76

TABLE 4. Data for the PDSs of fault f_1.

PDS Name	t_k (μs)	L_+ (km)
D	59.7	44.84
E	547.5	191.05
F	766.6	256.74
G	926.8	340.29
H	1405.6	448.25
I'	1187.9	383.01

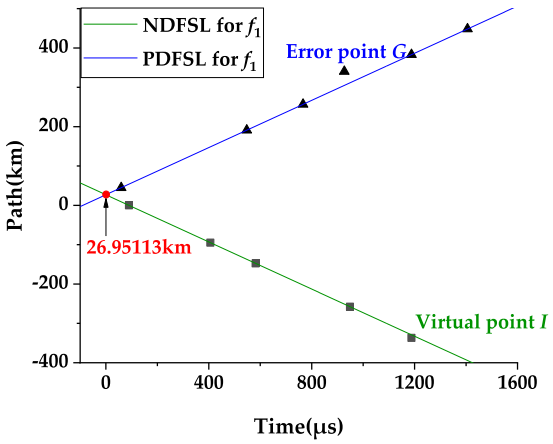

FIGURE 12. Diagram of two FSLs of fault f_1 for fault location.

the substation *C* records the error time which is 913.9μs. The traveling wave arrival time of each substation and its distance from the DBP are recorded according to this model, where the NDSs data and PDSs data are shown in Tables 5 and 6, respectively.

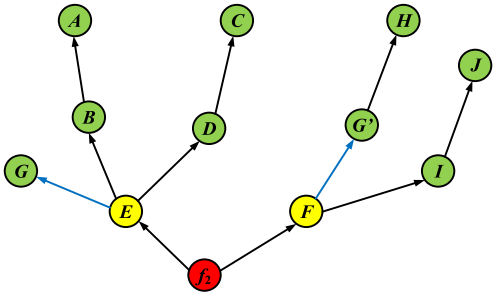

FIGURE 13. Directed tree model for fault f_2.

TABLE 5. Data for the NDSs of fault f_2.

NDS Name	t_k (μs)	L_- (km)
A	713.1	-174.19
B	537.2	-121.47
C	913.9	-191.05
D	619.7	-146.21
E	131.9	0
G	366.0	-247.42

TABLE 6. Data for the PDSs of fault f_2.

PDS Name	t_k (μs)	L_+ (km)
F	87.3	65.69
G'	366.0	149.24
H	Data missed	257.20
I	508.5	191.96
J	772.9	271.22

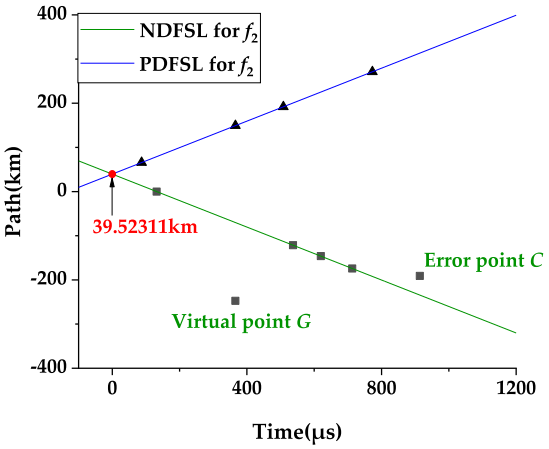

FIGURE 14. Diagram of two FSLs of fault f_2 for fault location.

According to the data in Tables 5 and 6 and the linear fitting principle, two FSLs called PDFSL and NDFSL are plotted in this rectangular coordinate system, as shown in Figure 14. The straight line equation of the two FSLs is calculated by the principle of univariate linear regression as follow:

$$\begin{cases} Y = -0.29971X + 39.51859 \\ Y = 0.29975X + 39.52764 \end{cases} \tag{21}$$

where $a_1 = 0.29971$, $a_2 = 0.29975$, $b_1 = -39.51859$ and $b_2 = 39.52764$.

In linear fitting, the error point C and the virtual point G are eliminated according to the correction criterion 1:

$$\begin{cases} \left|t'_C - t_C\right| = |769.3 - 913.9|\,\mu s = 144.6\mu s \geq 1\mu s \\ \left|t'_G - t_G\right| = |957.4 - 366.0|\,\mu s = 591.4\mu s \geq 1\mu s \end{cases} \tag{22}$$

where t_C' and t_G' are the fitting times of the fault traveling waves to the subtree nodes C and G, respectively. So that the incorrect virtual tree EG is eliminated. At this time, the slopes of the two fitted straight lines are satisfied by correction criterion 2:

$$\begin{cases} \left|\dfrac{|-a_1|}{v_{light}} - 1\right| \times 100\% = \left|\dfrac{|-0.29971|}{0.3} - 1\right| \\ \qquad \times 100\% = 0.097\% \leq 1\% \\ \left|\dfrac{|a_2|}{v_{light}} - 1\right| \times 100\% = \left|\dfrac{|0.29975|}{0.3} - 1\right| \\ \qquad \times 100\% = 0.083\% \leq 1\% \end{cases} \tag{23}$$

The location of the fault point is the intersection of two fitted straight lines. According to the Equations (13) and (21), the fault distance $l_{Ef2} = 39.52311$km. The location error of this case is 0.010%.

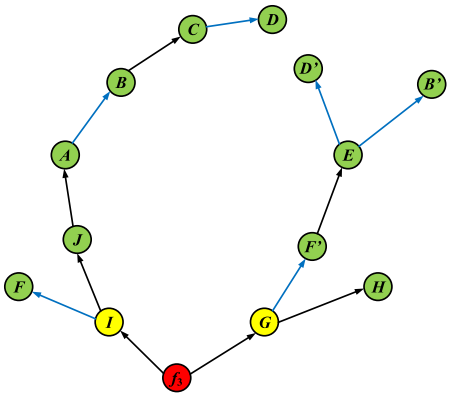

FIGURE 15. Directed tree model for fault f_3.

3) TEST CASE 3: BC FAULT f_3

In the third case, the BC fault f_3 shown in Figure 7 occurs on the line IG. Point I is selected as the DBP, and the direction of the wave velocity when the traveling wave is transmitted from the fault point f_3 to point G is set to the positive direction. A directed tree model for fault f_3 as shown in Figure 15 is established. Assume that, the traveling wave location device of the substation C fails or fails to start, which causes the arrival time of the traveling wave signal is not recorded. The traveling wave arrival time of each substation and its distance from the DBP are recorded according to this model, where the NDSs data and PDSs data are shown in Tables 7 and 8, respectively.

According to the data in Tables 7 and 8 and the linear fitting principle, two FSLs called PDFSL and NDFSL are plotted in this rectangular coordinate system, as shown in Figure 16.

TABLE 7. Data for the NDSs of fault f_3.

NDS Name	t_k (μs)	L_- (km)
A	860.7	-189.24
B	1036.7	-241.96
C	Data missed	-336.76
D	1302.0	-381.56
F	595.0	-126.27
I	229.4	0
J	493.7	-79.26

TABLE 8. Data for the PDSs of fault f_3.

PDS Name	t_k (μs)	L_+ (km)
B'	1036.7	434.23
D'	1302.0	458.97
E	814.1	312.76
F'	595.0	247.07
G	316.2	163.52
H	676.4	271.48

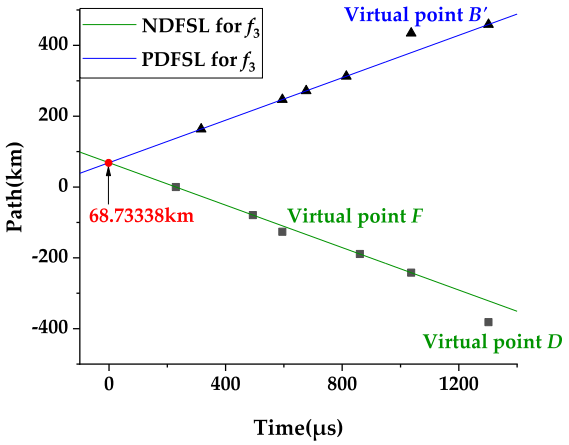

FIGURE 16. Diagram of two FSLs of fault f_3 for fault location.

The straight line equation of the two FSLs is calculated by the principle of univariate linear regression as follow:

$$\begin{cases} Y = -0.29970X + 68.72363 \\ Y = 0.29973X + 68.74314 \end{cases} \tag{24}$$

where $a_1 = 0.29970$, $a_2 = 0.29973$, $b_1 = -68.72363$ and $b_2 = 68.74314$.

In linear fitting, the virtual point D, virtual point F, and virtual point B' are eliminated according to the correction criterion 1:

$$\begin{cases} \left|t'_D - t_D\right| = |1502.5 - 1302.0|\,\mu s = 200.5\mu s \geq 1\mu s \\ \left|t'_F - t_F\right| = |650.6 - 595.0|\,\mu s = 55.6\mu s \geq 1\mu s \\ \left|t'_{B'} - t_{B'}\right| = |1219.4 - 1036.7|\,\mu s = 182.7\mu s \geq 1\mu s \end{cases} \tag{25}$$

where t_D', t_F' and $t_{B'}$' are the fitting times of the fault traveling waves to the subtree nodes D, F and B', respectively. So that the incorrect virtual trees CD, IF and EB' are eliminated. At this time, the slopes of the two fitted straight

lines are satisfied by correction criterion 2:

$$\begin{cases} \left|\dfrac{|-a_1|}{v_{light}}-1\right|\times 100\% = \left|\dfrac{|-0.29970|}{0.3}-1\right| \\ \qquad \times 100\% = 0.100\% \le 1\% \\ \left|\dfrac{|a_2|}{v_{light}}-1\right|\times 100\% = \left|\dfrac{|0.29973|}{0.3}-1\right| \\ \qquad \times 100\% = 0.090\% \le 1\% \end{cases} \tag{26}$$

The location of the fault point is the intersection of two fitted straight lines. According to the Equation (13) and (24), the fault distance $l_{If3} = 68.73338$km. The location error of this case is 0.004%.

4) TEST CASE 4: CG FAULT f_4

In the last case, the CG fault f_4 shown in Figure 7 occurs on the line AJ. Point A is selected as the DBP, and the direction of the wave velocity when the traveling wave is transmitted from the fault point f_4 to point J is set to the positive direction. A directed tree model for fault f_4 as shown in Figure 17 is established. It is assumed that the traveling wave location device of the substations D and G record the error times which are 1008.8μs and 538.6μs, respectively. The traveling wave arrival time of each substation and its distance from the DBP are recorded according to this model, where the NDSs data and PDSs data are shown in Tables 9 and 10, respectively.

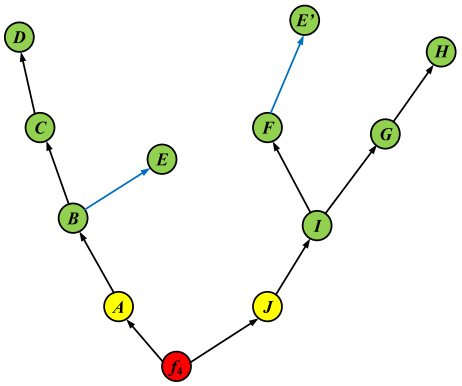

FIGURE 17. Directed tree model for fault f_4.

TABLE 9. Data for the NDSs of fault f_4.

NDS Name	t_k (μs)	L_- (km)
A	284.6	0
B	460.5	-52.72
C	776.8	-147.52
D	1008.8	-192.36
E	865.9	-174.19

According to the data in Tables 9 and 10 and the linear fitting principle, two FSLs called PDFSL and NDFSL are plotted in this rectangular coordinate system, as shown in Figure 18. The straight line equation of the two FSLs is calculated by the principle of univariate linear regression as follow:

TABLE 10. Data for the PDSs of fault f_4.

PDS Name	t_k (μs)	L_+ (km)
E'	865.9	381.20
F	768.0	315.51
G	538.6	352.76
H	1252.5	460.72
I	346.7	189.24
J	82.3	109.98

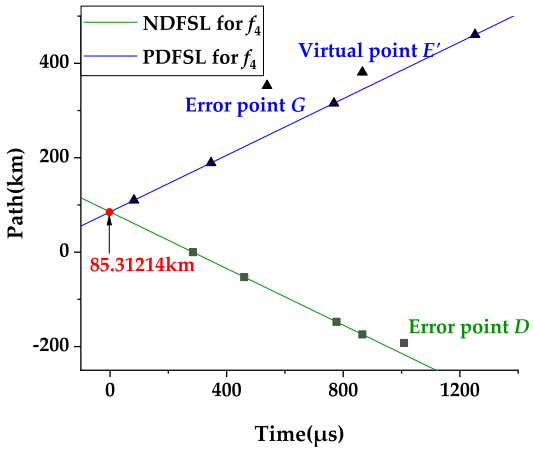

FIGURE 18. Diagram of two FSLs of fault f_4 for fault location.

$$\begin{cases} Y = -0.29969X + 85.29421 \\ Y = 0.29972X + 85.33009 \end{cases} \tag{27}$$

where $a_1 = 0.29969$, $a_2 = 0.29972$, $b_1 = -85.29421$ and $b_2 = 85.33009$.

In linear fitting, the error point D, error point G, and virtual point E' are eliminated according to the correction criterion 1:

$$\begin{cases} |t'_D - t_D| = |926.5 - 1008.8|\,\mu s = 82.3\mu s \ge 1\mu s \\ |t'_G - t_G| = |892.3 - 538.6|\,\mu s = 353.7\mu s \ge 1\mu s \\ |t'_{E'} - t_{E'}| = |987.2 - 865.9|\,\mu s = 121.3\mu s \ge 1\mu s \end{cases} \tag{28}$$

where t_D', t_G' and $t_{E'}$' are the fitting times of the fault traveling waves to the subtree nodes D, G and E', respectively. So that the incorrect virtual trees FE' is eliminated. At this time, the slopes of the two fitted straight lines are satisfied by correction criterion 2:

$$\begin{cases} \left|\dfrac{|-a_1|}{v_{light}}-1\right|\times 100\% = \left|\dfrac{|-0.29969|}{0.3}-1\right| \\ \qquad \times 100\% = 0.103\% \le 1\% \\ \left|\dfrac{|a_2|}{v_{light}}-1\right|\times 100\% = \left|\dfrac{|0.29972|}{0.3}-1\right| \\ \qquad \times 100\% = 0.093\% \le 1\% \end{cases} \tag{29}$$

The location of the fault point is the intersection of two fitted straight lines. According to Equations (13) and (27), the fault distance $l_{Af4} = 85.31214$km. The location error of this case is 0.002%.

TABLE 11. Fault location results.

Test Case	1	2	3	4
Fault Type	AG fault f_1	ABG fault f_2	BC fault f_3	CG fault f_4
Transition Resistance (Ω)	50	100	200	400
Fault Section	Line *CD*	Line *EF*	Line *IG*	Line *AJ*
Location Device Condition	*G* (TRE)	*C* (TRE); *H* (TWSND)	*C* (TWSND)	*D* (TRE); *G* (TRE)
Actual FD from DBP (km)	26.95114	39.52311	68.73338	85.31214
Calculated FD (km)	26.95	39.53	68.74	85.31
Error (%)	0.003	0.010	0.004	0.002

where TRE = Time Recording Error, TWSND = Traveling Wave Signal Not Detected and FD = Fault Distance.

TABLE 12. Compared results of the three methods.

Test Case	Actual FD from DBP (km)	Method in [25]		Method in [26]		The Proposed Method	
		Calculated FD (km)	Error (%)	Calculated FD (km)	Error (%)	Calculated FD (km)	Error (%)
1	26.95	26.95814	0.018	26.95944	0.021	26.95114	0.003
2	39.53	39.54061	0.016	39.52008	0.015	39.52311	0.010
3	68.74	68.72603	0.008	68.75520	0.009	68.73338	0.004
4	85.31	85.32059	0.010	85.31798	0.003	85.31214	0.002

D. PERFORMANCE EVALUATION OF PROPOSED METHOD

Table 11 is obtained from the simulation results in Section V.C. The results summarized in Table 11 show that the method proposed in this paper has high accuracy, small error, and only needs the intersection of two fitted straight lines to achieve fault location. The fault location idea is simple, convenient and feasible with a minor error of $<0.01\%$, for any fault section and fault type. Even if any location device in the power system faults startup failure or time recording error, highly accurate and reliable location results can still be obtained because the error point is effectively eliminated through the correction criteria in the proposed method.

In this paper, two traveling wave location methods for transmission networks based on network-wide information and capable of eliminating time recording errors are selected for the comparative study, where the processing time and sampling frequency are consistent with the simulation in proposed method, 10ms and 10MHz respectively. The Dijkstra algorithm is also used to find the shortest path of the fault traveling wave in the method of [26], but the method in [25] uses the Floyd algorithm to find the shortest path. According to the research in [26], in the case that complex ring networks are required to be decomposed into a radial network, the Floyd algorithm is not suitable, because data failure and miscalculation are occurred when the fault line is in the ring network. The methods of [25] and [26] both need to consider the impact of wave velocity on the calculation of the fault distance (set the wave velocity $v = 0.2997\mu s$ / km), and when the final fault distance is calculated, the entire network information is processed by weighting and summing the weights. It is easy to cause remote information with higher time accuracy ignored when setting weights, and more human interference factors are added. Therefore, the robustness and reliability of these two methods are not as excellent as the proposed method. The performance of the compared methods is listed in Table 12, where results show that the proposed method has slightly lower errors.

VI. CONCLUSION

A novel traveling wave fault location method based on directed tree model and linear fitting is proposed in this paper. Through theoretical analysis and simulation results, the complex engineering problems are transformed into intuitive mathematical problems by this method, which achieves high-precision and reliable location after any transmission line faults in the entire transmission network. The advantages of this method are as follows:

(1) All the recorded data are plotted in the rectangular coordinate system. It is not necessary to judge whether each detection data is correct in sequence, because time recording error points are automatically eliminated during linear fitting. The accuracy of fault location is not affected by time unrecorded and recording error points, with high fault tolerance rate.

(2) In this proposed method, traveling wave velocity is only used as the slope of two FSLs in linear regression analysis, and its size does not need to be considered affected by other factors, according to the characteristic that fault traveling wave transmission distance is proportional to the transmission time. Therefore, the problem of the impact of wave velocity uncertainty on the accuracy of fault location in traveling wave location is solved, and the fault distance is obtained simply and intuitively through the intersection of two FSLs.

(3) In this proposed method, the erroneous data points, which represents the non-shortest transmission path of the fault traveling wave, are automatically eliminated, and the fault information of the entire transmission network in fault location is comprehensively utilized, according to the FSL in the directed tree model. The problem of difficult fault location due to the complex traveling wave transmission path in the transmission network with ring network is solved, because the ring network is automatically unlooped which reduces the steps of setting data and enables easier fault location.

(4) In order to ensure the accuracy of fault location in this method, two correction criteria are set in the process of linear

error elimination of erroneous data points. The correction criterion 1 $|t_k'\text{-}t_k| \leq 1\mu$s, the setting of 1μs basically guarantee that the location error is within 150m. When the slope of the FSL is satisfied by the correction criterion 2 $|(|a|/v_{light})\text{-}1|\times 100\% \leq 1\%$, the location accuracy of the method is ensured, based on the analysis of the transmission characteristics of the traveling wave. The location accuracy error is less than 0.01% for any fault section and fault type. Even if any location device in the power system faults startup failure or time recording error, highly accurate and reliable location results can still be obtained.

REFERENCES

[1] M. Korkali, H. Lev-Ari, and A. Abur, "Traveling-wave-based fault-location technique for transmission grids via wide-area synchronized voltage measurements," *IEEE Trans. Power Syst.*, vol. 27, no. 2, pp. 1003–1011, May 2012.

[2] H. Liang, Y. Liu, G. Sheng, and X. Jiang, "Reproduction methodology for single Phase-to-Ground faults in overhead transmission lines," *IEEE Access*, vol. 5, pp. 17403–17413, 2017.

[3] D. Tzelepis, G. Fusiek, A. Dysko, P. Niewczas, C. Booth, and X. Dong, "Novel fault location in MTDC grids with non-homogeneous transmission lines utilizing distributed current sensing technology," *IEEE Trans. Smart Grid*, vol. 9, no. 5, pp. 5432–5443, Sep. 2018.

[4] R. Chen, X. Yin, X. Yin, Y. Li, and J. Lin, "Computational fault time difference-based fault location method for branched power distribution networks," *IEEE Access*, vol. 7, pp. 181972–181982, 2019.

[5] R. Krishnathevar and E. E. Ngu, "Generalized impedance-based fault location for distribution systems," *IEEE Trans. Power Del.*, vol. 27, no. 1, pp. 449–451, Jan. 2012.

[6] Y. Xi, Y. Cui, X. Tang, Z. Li, and X. Zeng, "Fault location of lightning strikes using residual analysis based on an adaptive Kalman filter," *IEEE Access*, vol. 7, pp. 88126–88137, 2019.

[7] T. A. Alexopoulos, N. M. Manousakis, and G. N. Korres, "Fault location observability using phasor measurements units via semidefinite programming," *IEEE Access*, vol. 4, pp. 5187–5195, 2016.

[8] N. Safari-Shad, R. Franklin, A. Negahdari, and H. A. Toliyat, "Adaptive 100% injection-based generator stator ground fault protection with real-time fault location capability," *IEEE Trans. Power Del.*, vol. 33, no. 5, pp. 2364–2372, Oct. 2018.

[9] R. J. Hamidi and H. Livani, "Traveling-wave-based fault-location algorithm for hybrid multiterminal circuits," *IEEE Trans. Power Del.*, vol. 32, no. 1, pp. 135–144, Feb. 2017.

[10] R. Benato, S. D. Sessa, M. Poli, C. Quaciari, and G. Rinzo, "An online travelling wave fault location method for unearthed-operated high-voltage overhead line grids," *IEEE Trans. Power Del.*, vol. 33, no. 6, pp. 2776–2785, Dec. 2018.

[11] C. Zhang, G. Song, T. Wang, and L. Yang, "Single-ended traveling wave fault location method in DC transmission line based on wave front information," *IEEE Trans. Power Del.*, vol. 34, no. 5, pp. 2028–2038, Oct. 2019.

[12] F. V. Lopes, B. F. Kusel, and K. M. Silva, "Traveling wave-based fault location on half-wavelength transmission lines," *IEEE Latin Amer. Trans.*, vol. 14, no. 1, pp. 248–253, Jan. 2016.

[13] Y. Xi, X. Zhang, Z. Li, X. Zeng, X. Tang, Y. Cui, and H. Xiao, "Double-ended travelling-wave fault location based on residual analysis using an adaptive EKF," *IET Signal Process.*, vol. 12, no. 8, pp. 1000–1008, Oct. 2018.

[14] F. V. Lopes, K. M. Dantas, K. M. Silva, and F. B. Costa, "Accurate two-terminal transmission line fault location using traveling waves," *IEEE Trans. Power Del.*, vol. 33, no. 2, pp. 873–880, Apr. 2018.

[15] A. Ghorbani and H. Mehrjerdi, "Negative-sequence network based fault location scheme for double-circuit multi-terminal transmission lines," *IEEE Trans. Power Del.*, vol. 34, no. 3, pp. 1109–1117, Jun. 2019.

[16] L. Yuansheng, W. Gang, and L. Haifeng, "Time-domain fault-location method on HVDC transmission lines under unsynchronized two-end measurement and uncertain line parameters," *IEEE Trans. Power Del.*, vol. 30, no. 3, pp. 1031–1038, Jun. 2015.

[17] R. Liang, Z. Yang, N. Peng, C. Liu, and F. Zare, "Asynchronous fault location in transmission lines considering accurate variation of the ground-mode traveling wave velocity," *Energies*, vol. 10, no. 12, p. 1957, Nov. 2017.

[18] D. Wang, Y. Ning, and C. Zhang, "An effective ground fault location scheme using unsynchronized data for multi-terminal lines," *Energies*, vol. 11, no. 11, p. 2957, Oct. 2018.

[19] R. Liang, N. Peng, L. Zhou, X. Meng, Y. Hu, Y. Shen, and X. Xue, "Fault location method in power network by applying accurate information of arrival time differences of modal traveling waves," *IEEE Trans. Ind. Informat.*, vol. 16, no. 5, pp. 3124–3132, May 2020.

[20] Y. Ning, D. Wang, Y. Li, and H. Zhang, "Location of faulty section and faults in hybrid multi-terminal lines based on traveling wave methods," *Energies*, vol. 11, no. 5, p. 1105, May 2018.

[21] J. Ding, X. Wang, Y. Zheng, and L. Li, "Distributed traveling-wave-based fault-location algorithm embedded in multiterminal transmission lines," *IEEE Trans. Power Del.*, vol. 33, no. 6, pp. 3045–3054, Dec. 2018.

[22] M. Pourahmadi-Nakhli and A. A. Safavi, "Path characteristic frequency-based fault locating in radial distribution systems using wavelets and neural networks," *IEEE Trans. Power Del.*, vol. 26, no. 2, pp. 772–781, Apr. 2011.

[23] S. Lan, M.-J. Chen, and D.-Y. Chen, "A novel HVDC double-terminal non-synchronous fault location method based on convolutional neural network," *IEEE Trans. Power Del.*, vol. 34, no. 3, pp. 848–857, Jun. 2019.

[24] F. Deng, X. Zeng, C. Yuan, X. Qin, and Z. Wu, "Novel traveling wave location algorithm for transmission network based on information fusion technology," in *Proc. Int. Conf. Intell. Comput. Technol. Autom. (ICICTA)*, Hunan, China, Oct. 2008, pp. 1091–1095.

[25] X. Zeng, N. Chen, Z. Li, and F. Deng, "Network-based algorithm for fault location with traveling wave," *Proc. CSEE*, vol. 28, no. 31, pp. 48–53, 2008.

[26] Z. Li, P. Tang, and X. Zeng, "Method of traveling wave fault location based on Dijkstra algorithm in power grid," *Autom. Electr. Power Syst.*, vol. 42, no. 18, pp. 162–168, 2018.

[27] O. V. Gnana Swathika and S. Hemamalini, "Prims-aided dijkstra algorithm for adaptive protection in microgrids," *IEEE J. Emerg. Sel. Topics Power Electron.*, vol. 4, no. 4, pp. 1279–1286, Dec. 2016.

[28] P. A. Crossley, "Time synchronization for transmission substations using GPS and IEEE 1588," *CSEE J. Power Energy Syst.*, vol. 2, no. 3, pp. 91–99, Sep. 2016.

[29] H. J. Vermeulen, L. R. Dann, and J. van Rooijen, "Equivalent circuit modelling of a capacitive voltage transformer for power system harmonic frequencies," *IEEE Trans. Power Del.*, vol. 10, no. 4, pp. 1743–1749, Oct. 1995.

[30] X. Dong, J. Wang, S. Shi, B. Wang, B. Dominik, and M. Redefern, "Traveling wave based single-phase-to-ground protection method for power distribution system," *CSEE J. Power Energy Syst.*, vol. 1, no. 2, pp. 75–82, Jun. 2015.

[31] S. Shi, B. Zhu, A. Lei, and X. Dong, "Fault location for radial distribution network via topology and reclosure-generating traveling waves," *IEEE Trans. Smart Grid*, vol. 10, no. 6, pp. 6404–6413, Nov. 2019.

[32] S. Mallat and W. L. Hwang, "Singularity detection and processing with wavelets," *IEEE Trans. Inf. Theory*, vol. 38, no. 2, pp. 617–643, Mar. 1992.

[33] S. Mallat and S. Zhong, "Characterization of signals from multiscale edges," *IEEE Trans. Pattern Anal. Mach. Intell.*, vol. 14, no. 7, pp. 710–732, Jul. 1992.

KUN YU received the M.S. degree from the Changsha University of Science and Technology, in 2014, and the Ph.D. degree from the Huazhong University of Science and Technology, Wuhan, in 2017. His research interest includes power system protection and control.

JUPENG ZENG received the B.E. degree from the Changsha University of Science and Technology, Changsha, China, in 2019, where he is currently pursuing the master's degree in electrical engineering. His research interest includes power system protection and control.

XIANGJUN ZENG (Senior Member, IEEE) received the bachelor's degree from Hunan University, in 1993, the M.Sc. degree from Wuhan University, in 1996, and the Ph.D. degree from the Huazhong University of Science and Technology, in 2001. He is currently a Professor with the Changsha University of Science and Technology. His research interest includes real-time computer applications in power systems control and protection.

FAN XU received the B.E. degree from the Hunan University of Technology, Zhuzhou, China, in 2019. She is currently pursuing the master's degree in electrical engineering with the Changsha University of Science and Technology. Her research interest includes power system protection and control.

YONG YE received the B.E. degree from the Changsha University of Science and Technology, Changsha, China, in 2018, where he is currently pursuing the master's degree in electrical engineering. His research interest includes power system protection and control.

YANRU NI received the master's degree from the Changsha University of Science and Technology, Changsha, China, in 2019, where she is currently pursuing the Ph.D. degree in electrical engineering. Her research interest includes power system protection and control.